EVOLUTIONARY BIOLOGY

Progressive decline in old pole gene expression signal enhances phenotypic heterogeneity in bacteria

Audrey M. Proenca*, Murat Tuğrul, Arpita Nath, Ulrich K. Steiner*

Cell growth and gene expression are heterogeneous processes at the single-cell level, leading to the emergence of multiple physiological states within bacterial populations. Aging is a known deterministic driver of growth asymmetry; however, its role in gene expression heterogeneity remains elusive. Here, we show that aging mother cells undergo a progressive decline in old pole activity, generating asymmetry in protein partitioning, gene expression, and cell morphology. We demonstrate that mother cells, when compared to their daughters, exhibit lower product inheritance and gene expression rates independently of promoter dynamics. The declining activity of maternal old poles generates gene expression gradients that manifest as mother-daughter asymmetry upon division, showing that asymmetry is progressively built over time within the maternal intracellular environment. Moreover, old pole aging correlates with a gradual increase in cell length, leading to morphological asymmetry. These findings provide further evidence for aging as a mechanism to enhance phenotypic heterogeneity in bacterial populations, with possible consequences for stress response and survival.

INTRODUCTION

Within isogenic populations, individual cells exhibit phenotypic heterogeneity in various aspects of their physiology, such as gene expression, protein partitioning, and growth rates. This variability often results from stochastic fluctuations that propagate across regulatory networks (*1*, *2*), leading to the coexistence of distinct metabolic states within a population (*3*, *4*). In bacterial populations, for instance, such gene expression fluctuations can lead some individuals to reproduce more quickly, while others enter a slow-growing or dormant state (*5*). Rather than being detrimental, this physiological heterogeneity is closely tied to survival in stressful conditions or rapidly changing environments (*6*–*8*). Nonetheless, recent studies have demonstrated that deterministic factors, such as cellular aging, also contribute toward the phenotypic heterogeneity previously attributed to stochasticity alone (*9*–*12*).

Aging, a physiological decline over time (*13*, *14*), propagates along bacterial lineages across generations. According to the classic evolutionary theory, aging should require a clear separation between the soma and germline (*15*). The fact that many bacteria divide with morphological symmetry has, consequently, led to the assumption that these organisms should flee aging (*15*–*17*). Nevertheless, the last decades have gathered broad evidence that aging occurs in unicellular organisms such as yeast (*18*), algae (*19*), and bacteria (*20*, *21*), indicating that even a slight asymmetry between parent and offspring is sufficient for aging to evolve (*22*). In *Escherichia coli*, which divide with apparent morphological symmetry, aging is determined by the asymmetric inheritance of cell poles. Rod-shaped bacteria synthesize a new pole at the central plane after each fission. In the following division, one cell inherits this new pole, while the other receives an old pole that can be passed over many generations (Fig. 1A). The deterministic inheritance of old poles is associated with reduced growth, lower division rates, and increased mortality, whereas the inheritance of new poles leads to higher fitness (*11*, *20*, *21*, *23*). This physiological heterogeneity contributes to the variance in lifespan among cells of identical genetic background (*24*) and can determine differential survival under sustained stress (*11*, *25*). It is therefore reasonable to assume that old pole cells progressively accumulate an "aging factor," which is asymmetrically partitioned upon division (*26*–*28*). This process can be described as a mother cell that ages by retaining the old pole while producing rejuvenated daughter cells with each division. Here, we will adhere to this perspective, as it refers back to the concept of separation between soma and germline (*29*) and simplifies the definition of aging at the single-cell level.

A possible mechanism of bacterial aging is the asymmetric partitioning of intracellular damage (*23*, *30*, *31*). Aggregates of misfolded proteins, for instance, tend to accumulate in old cell poles through processes of nucleoid exclusion (*32*–*35*). The continuous inheritance of protein aggregates by the mother cell negatively correlates with growth rates (*32*, *36*). This mechanism traces an important parallel with eukaryotic aging hallmarks (*37*), since protein misfolding is the basis of many age-associated diseases (*33*, *38*), and the asymmetric partitioning of damaged proteins is essential for stem cell maintenance (*39*). However, more recent studies suggest that other factors must be involved in bacterial aging. Large protein aggregates are generally absent in unstressed populations (*40*), and yet the physiological distinction between mothers and daughters is observed in healthy cells (*10*, *41*). In addition, for cells under heat stress, the rejuvenation of the daughter depends on the chronological age of the mother (*11*), indicating that daughters can inherit intracellular damage not associated with old poles. These results suggest that, besides damage partitioning, other intracellular mechanisms also contribute to the physiological asymmetry between mother and daughter cells.

Sources of physiological heterogeneity that are considered purely stochastic can provide hints of mechanisms that influence bacterial aging (*42*). For example, the partitioning of freely diffusing proteins upon division is regarded as a highly stochastic process (*2*), but recent evidence suggests that newly synthesized gene products are partitioned with deterministic asymmetry toward daughter cells (*43*). These results, however, were limited to early divisions. It remains unclear

Institute of Biology, Evolutionary Demography Group, Freie Universität Berlin, Königin-Luise-Str. 1-3, 14195 Berlin, Germany.
*Corresponding author. Email: aproenca@zedat.fu-berlin.de (A.M.P.); ulrich.steiner@fu-berlin.de (U.K.S.)

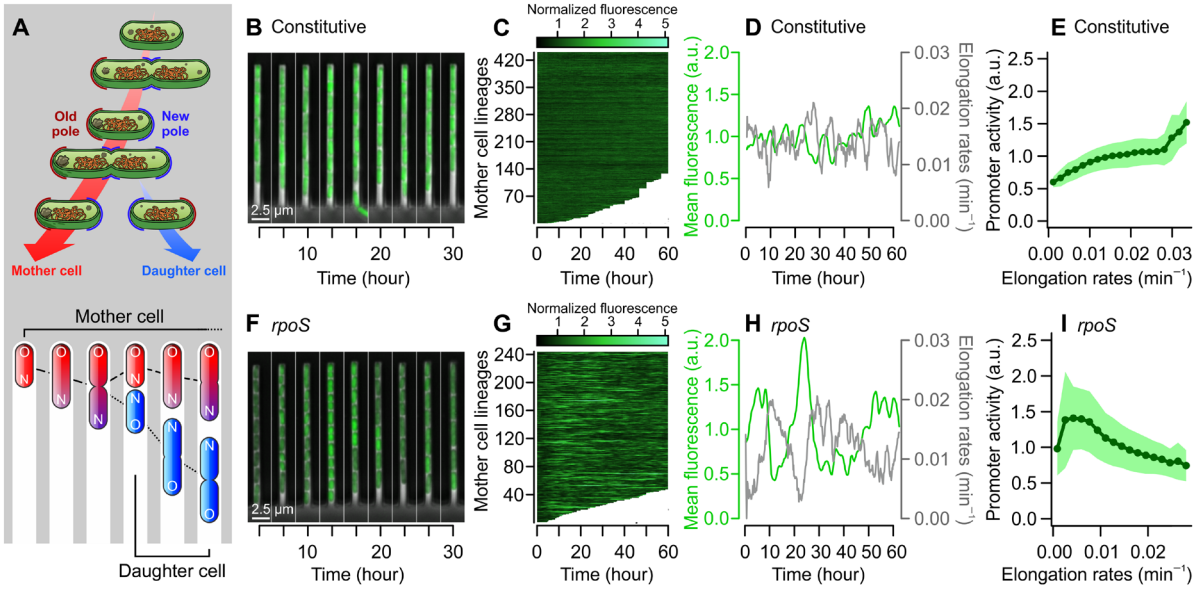

Fig. 1. Gene expression stochasticity and correlation with growth demonstrate contrasting promoter dynamics. (**A**) Graphical representation of bacterial aging through asymmetric pole inheritance (top) and cells growing in the mother machine device (bottom). Old cell poles, inherited by mother cells with each division, remain trapped at the closed end of growth wells. When the mother divides, it produces a daughter cell that inherits its new pole. To investigate whether this asymmetry impacts gene expression across generations, we tracked bacteria expressing GFP from promoters with contrasting dynamics. (**B** to **D**) Mother cells constitutively expressing GFP showed little fluctuation in fluorescence levels over time. (**E**) Across the population (n = 62,533 cell divisions), cells exhibited a positive correlation between elongation rates and constitutive promoter activity (Pearson's correlation coefficient = 0.298 and $P < 0.001$). In contrast, (**F** to **H**) mother cells expressing GFP from the *rpoS* promoter showed highly stochastic transcriptional bursts that coincided with periods of slower growth (see also fig. S1). (**I**) This pattern was also present across the whole population, with slow-growing cells displaying high *rpoS* promoter activity (n = 42,350 observations; Pearson's correlation coefficient = −0.393 and $P < 0.001$). Bins = mean ± SD. Mother cells in (C) and (G) were sorted by longevity, with interrupted lines representing cells that died or were washed away.

whether asymmetry increases as a function of maternal age and how this pattern develops intracellularly across generations. Moreover, gene expression stochasticity propagates across regulatory networks, leading to heterogeneity at the single-cell level (*2*, *8*, *44*). It is therefore essential to determine whether mother and daughter cells show asymmetric rates of gene expression rather than just an asymmetric inheritance of products. If divisional asymmetry develops over time and its impact can be extended to gene expression, this could reveal another mechanism of bacterial aging.

Here, we investigate the contribution of aging to phenotypic heterogeneity by quantifying asymmetry in growth, gene expression, and protein partitioning across generations. Independently of the underlying promoter dynamics, we found that mother cells display lower rates of both gene expression and product inheritance. Mother-daughter asymmetry is present from the early maturation of an old pole and increases with maternal aging, thus propagating over each cell division. We show that this asymmetry originates from intracellular gradients formed within the mother cell before division, as a function of a progressive decline in old pole protein concentration. Daughter cells do not exhibit such decline: From birth to division, they show a homogeneous intracellular environment. Moreover, we demonstrate that this decline in old pole activity corresponds to a progressive increase in maternal cell length, leading to the emergence of morphological asymmetry in aging lineages. Thus, with each cell division, aging enhances the phenotypic heterogeneity found in bacterial populations, creating deterministic asymmetric patterns in growth, product partitioning, gene expression, and cell morphology.

RESULTS

Promoter dynamics vary in noise and correlation with growth

To evaluate the contribution of aging to phenotypic heterogeneity at the single-cell level, we investigated cell growth, inheritance of gene products, and gene expression variability. Using time-lapse microscopy, we imaged *E. coli* cells to quantify these aspects of bacterial physiology and their interactions over time. To follow mother and daughter cells across generations, we cultured lineages growing in constant exponential phase within mother machine devices (*45*). This microfluidics design contains thousands of growth wells connected to wide flow channels, which supply fresh nutrients to trapped cells (Fig. 1A). The mother cell remains lodged at the closed end of a growth well, while continuously producing daughter cells. Early tests have shown that diffusion within these wells occurs faster than nutrient uptake (*45*), ensuring that mothers and daughters experience the same nutritional conditions. From the resulting images, we tracked mother cells for up to 100 generations and each daughter from birth to its first division, quantifying aspects of their growth physiology (length, division intervals, and elongation rates) and gene expression (mean fluorescence intensity and promoter activity).

We measured gene expression in strains containing a promoter of interest fused to fluorescent transcriptional reporters (movie S1). For this, we used two promoters with contrasting dynamics: *rpoS* (*46*) and a constitutive promoter PA1 (*47*). The former expresses the RpoS sigma factor, which regulates the general stress response and the transition to stationary phase (*48*, *49*), showing highly stochastic expression in transcriptional bursts that negatively correlate with

growth rates (*4*, *8*). The constitutive promoter, on the other hand, is expected to show a positive correlation between expression and growth (*50*) and lower noise levels than *rpoS* (*1*). By comparing the long-term activity of both reporters, we can identify effects of aging that are independent of specific promoter dynamics.

We first set out to confirm that both reporters exhibited the predicted promoter dynamics. For this, we quantified the mean fluorescence of each mother cell lineage over time. As predicted, *rpoS* exhibited highly stochastic fluctuations, showing larger variance than the constitutive promoter (*F* test: $F = 4.53$ and $P < 0.001$). This difference in noise levels can be expressed by coefficients of variation (CV), with the constitutive reporter showing a twofold lower CV = 20.43% (Fig. 1, B to D) than *rpoS* (CV = 43.49%; Fig. 1, F to H). When we considered the rate of expression of each reporter (see Materials and Methods for details), the constitutive promoter showed an increase in activity with faster elongation rates (Fig. 1E and fig. S1). In contrast, random bursts of *rpoS* expression corresponded to periods of slower growth (Fig. 1H and fig. S1), with the relationship between elongation rates (r) and promoter activity being expressed by an exponential decay function ($1.50*e^{-28.90*r}$; Fig. 1I). Since few cells undergo large transcriptional bursts, *rpoS* measurements yielded long-tailed distributions of mean fluorescence and promoter activity, in contrast with the Gaussian distribution of constitutively expressed green fluorescent protein (GFP; fig. S1).

These results confirm the expectations for both promoters, summarizing the opposite dynamics of *rpoS* and constitutive reporters in terms of noise and growth dependence. We performed additional controls to confirm that the *rpoS* reporter reflects the expected biological activity of this transcription factor, with its transcription levels increasing as cells enter stationary phase (fig. S2). While these observations demonstrate that bacterial populations have high cell-to-cell variance in gene expression, the next section will show that part of this heterogeneity can be attributed to underlying cellular aging processes.

Asymmetric product partitioning is independent of expression dynamics

The asymmetric metabolic rates of *E. coli* can be represented through a quantification of elongation rates over each generation (Fig. 2A). Daughter cells displayed faster growth than mother cells, with their generation times being, on average, 1.81 min shorter (paired *t* tests; constitutive: $t = 26.24$, $n = 31{,}019$, and $P < 0.001$; and *rpoS*: $t = 19.98$, $n = 21{,}161$, and $P < 0.001$). We can expect this asymmetry to be reflected also in gene expression. For example, previous results have shown that gene products are inherited asymmetrically during the early formation of microcolonies (*43*). The long-term dynamics of this asymmetry, however, must be evaluated to determine how aging shapes the heterogeneity of a population. Furthermore, to generalize these previous findings, we must investigate whether this pattern remains true when expression is negatively correlated with metabolic rates, as in the case of the *rpoS* reporter. Since RpoS has growth-inhibitory activity, it might be more prevalent in mother cells than in their faster-growing daughters.

To verify this, we measured fluorescence asymmetry shortly after each division. Daughter cells showed higher mean fluorescence levels for both reporters (Fig. 2B), with GFP inheritance becoming slightly more asymmetric over time (Fig. 2C). Therefore, the mother cell retains a lower concentration of expressed proteins independently of the underlying promoter dynamics. We further investigated the role of asymmetry in determining fluorescence levels through simple

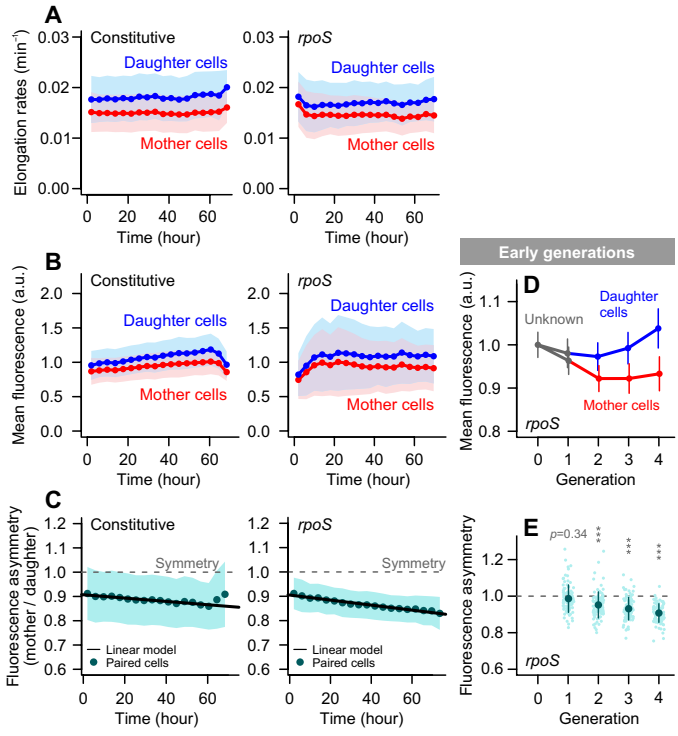

Fig. 2. Mother and daughter cells show asymmetry in growth and gene product inheritance. (**A**) Daughter cells displayed faster growth, with a stable asymmetry in elongation rates over time (paired *t* tests; constitutive: $t = 174.42$, $n = 31{,}019$, and $P < 0.001$; and *rpoS*: $t = 132.95$, $n = 21{,}161$, and $P < 0.001$). (**B**) Independently of the underlying promoter dynamics shown in Fig. 1, mother cells exhibited lower mean fluorescence levels after division (paired *t* tests; constitutive: $t = 189.21$, $n = 31{,}019$, and $P < 0.001$; and *rpoS*: 272.76, $n = 18{,}452$, and $P < 0.001$). This supports prior reports that *E. coli* partitions "good" components asymmetrically upon division (*43*, *51*). (**C**) Mother-daughter asymmetry exhibited a slight increase with maternal age, which was verified for both the constitutive (*slope* = −0.0006 and $P < 0.001$) and *rpoS* promoters (*slope* = −0.001 and $P < 0.001$). [(A) to (C)] Bins = mean ± SD. (**D**) Asymmetry was absent on the first division observed within the mother machine, since the founder cell has equal probability of being a mother or a daughter. Nonetheless, it appears once the inheritance of old poles becomes established, showing that aging effects quickly emerge along the following generations. Bins = mean ± SEM. (**E**) Early generations had significant asymmetry from the second generation onward (***$P < 0.001$, with Bonferroni correction).

statistical models (table S1), estimating the contribution of several predictors to the total variance in fluorescence signal. The partitioning of GFP molecules is a highly stochastic process, with unexplained variance accounting for 54.1% of the total heterogeneity for both reporters. Elongation rates accounted for most of the explained heterogeneity of *rpoS* fluorescence ($V_r = 23.5\%$), a pattern that was not verified for constitutive GFP expression ($V_r = 1.6\%$). Last, in both cases, the age category of a cell (whether it is a mother or a daughter) had a similar contribution to the total variance ($V_{asym} = 9.9$ and 11.8%), suggesting that mother-daughter asymmetry increases the total heterogeneity of a population.

Despite the contribution of asymmetry for heterogeneity and its increase with maternal age, we must consider that substantially old mother cells are a rare occurrence outside of a mother machine device. To ensure that this effect is relevant for bacterial populations in general, we must determine how quickly age-associated differences in protein

inheritance appear. We investigated this by quantifying *rpoS* asymmetry for the earliest generations recorded within the device (Fig. 2, D and E). Because the polarity of the "founder" cell is unknown, the cell at the closed end has a 50% probability to inherit either a new or old pole. If the asymmetry observed in Fig. 2B has a physiological origin, it should be absent at this first generation. As shown in Fig. 2D, asymmetric fluorescence levels were not verified in the first division, and gradually appeared along subsequent generations. Because first-generation cells are subjected to the same positioning biases as mothers and daughters, these results also indicate that asymmetry is due to aging rather than a positioning artifact (see Supplementary Text and figs. S3 and S4 for details and further controls).

Together, these results suggest that asymmetric protein partitioning is a consequence of bacterial aging. This phenomenon manifests independently of the stochastic processes affecting specific promoters and their relationship with elongation rates. We show that asymmetric physiology arises in early generations due to the inheritance of old poles, in agreement with studies describing this process in agarose pads (*21*, *43*). Moreover, this asymmetry is amplified with maternal age, thus propagating along cell lineages and enhancing the phenotypic heterogeneity of a population upon each division.

Aging contributes to gene expression heterogeneity

We next investigated whether aging leads to asymmetry in gene expression levels. While the asymmetric distribution of proteins shown in Fig. 2 contributes to cell-to-cell heterogeneity, it does not suffice to determine whether these products are synthesized at asymmetric rates. This additional layer of metabolic asymmetry would imply a deeper physiological difference between mothers and daughters. To verify this, we calculated the rate of GFP production from each promoter, taking into consideration differences in individual growth rates (*4*, *8*). This correction is essential because daughter cells elongate faster and have a larger ribosomal content than mother cells (*51*), which would otherwise generate confounding effects.

Even after accounting for the underlying asymmetry in metabolic rates, we found that daughter cells had larger rates of constitutive fluorescence expression (Fig. 3A). As for *rpoS* expression, we expected to find higher promoter activity among mother cells, since RpoS has growth-inhibitory activity. Instead, we verified that daughter cells had greater *rpoS* expression. Moreover, mothers and daughters had asymmetric gene expression even when growing at similar rates (Fig. 3B). We evaluated the relationship between elongation rates, gene expression, and asymmetry through analyses of covariance (ANCOVA) for each promoter. Constitutive promoter activity increased with growth ($t = 30.25$ and $P < 0.001$) with a similar slope for both mother and daughter cells (*slope* = 1.94 and ANCOVA interaction, $P = 0.084$), but daughters showed higher expression rates ($t = 17.47$ and $P < 0.001$). The *rpoS* promoter exhibited similar asymmetric activity ($t = 23.21$ and $P < 0.001$), with a steeper negative correlation between growth and expression observed among mother cells (*slope* = −49.56 and $P < 0.001$) than daughter cells (*slope* = −46.53 and $P < 0.001$). Since elongation rates are highly correlated with ribosomal content (*52*, *53*), these results suggest that the aging effects we observed are not produced by the asymmetric inheritance of ribosomes (*51*).

Therefore, bacterial asymmetry extends to both processes of protein partitioning and gene expression. Daughter cells not only inherit more new products but also produce them at a higher rate. Since gene expression asymmetry could not be explained solely by a difference in metabolic rates, this suggests that other intracellular processes associated with aging might contribute to this deterministic heterogeneity.

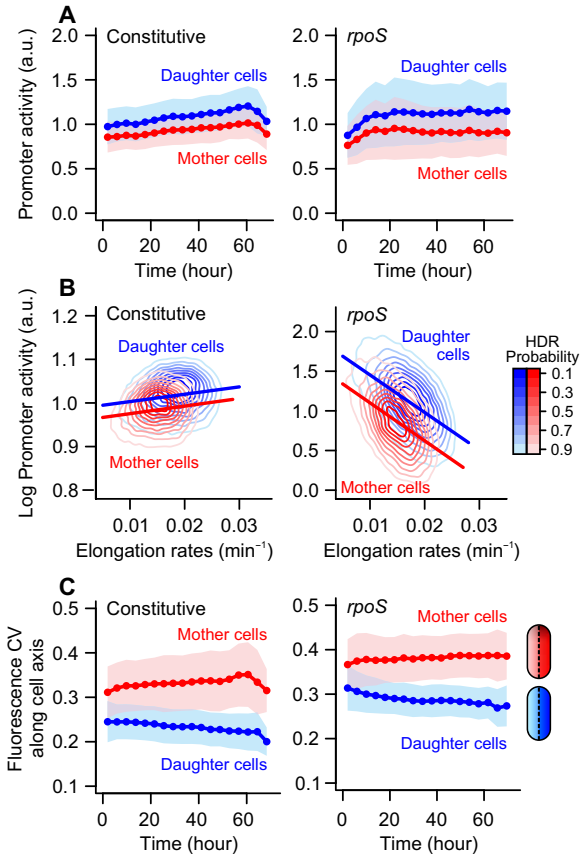

Fig. 3. Aging leads to gene expression asymmetry independently of promoter dynamics. (**A**) Daughter cells exhibited higher promoter activity, whether the overall activity levels remained constant or increased over time (paired *t* test; constitutive: $t = 185.14$, $n = 31{,}019$, and $P < 0.001$; and *rpoS*: $t = 209.72$, $n = 18{,}452$, and $P < 0.001$). This indicates that, besides simply inheriting more newly synthesized products, daughter cells have higher gene expression rates. (**B**) Gene expression asymmetry was present independently of its correlation with elongation rates. This correlation was better represented by separate regression lines for mothers and daughters, suggesting that even cells growing at a similar rate show asymmetric gene expression. Thus, the difference in promoter activity cannot be explained solely by the difference in metabolic rates shown in Fig. 2A. Data distribution is shown through outlined areas representing the highest density regions for the given probabilities. (**C**) Examining the intracellular distribution of fluorescence levels, mothers and daughters also differed in the variance of fluorescence signals. [(A) and (C)] Bins = mean ± SD.

To examine potential sources of asymmetry at the intracellular level, we asked whether mother and daughter cells differed in the intracellular distribution of synthesized products. For this, we quantified the variance in gene products across the length of each cell (i.e., from old to new pole). Independently of the reporter, we observed that mothers harbored much larger intracellular variation than their daughters (Fig. 3C; ANCOVA, $P < 0.001$). This distinction increased with maternal age, with the CV of mother cells increasing over time (constitutive: $t = 23.92$ and $P < 0.001$; and *rpoS*: $t = 13.21$ and $P < 0.001$), while the fluorescence variance within daughter cells decreased (constitutive: $t = -33.99$ and $P < 0.001$; and *rpoS*: $t = -34.55$ and $P < 0.001$). This difference in intracellular fluorescence variance

might help elucidate the sources of asymmetry in gene expression and will be further explored in the following section.

Mother-daughter asymmetry is built within the mother cell

To further investigate the factors shaping intracellular variance in gene expression, we quantified the mean fluorescence signal along the cell axis of each individual. To allow for a comparison of these distributions, we normalized cells by length and calculated the average fluorescence transect for each generation (Fig. 4). To avoid biases introduced by positioning artifacts, we performed control analyses and corrections described in the Supplementary Materials (Supplementary Text and fig. S5).

The resulting transects indicated that the intracellular variance found in mother cells derives from a gradient in gene expression between new and old poles (Fig. 4, A and B). We used generalized additive models to analyze these fluorescence gradients, considering the passage of time (in generations) and the distance from each pole to the center of the cell (as if the cell were cut in half). This allows us to determine whether aging changes either side of the cell differently, which would influence the formation of intracellular gradients. A graphical representation of these models is given in fig. S6, and the statistical output is detailed in tables S2 and S3. For both promoters, our analysis indicated that the effect of pole distance on fluorescence varied over time ($P < 0.001$). Comparing the two halves of the mother cell, we observed that expression levels varied differently over time ($P < 0.001$) and across the cell length ($P < 0.001$) for new and old halves. In other words, maternal fluorescence levels declined from the center toward the cell poles, with a much sharper decline observed in the old half of the cell (fig. S6, A and B). This pattern became more pronounced over generations, with the old half growing darker as the mother aged. Together, these factors explained 51.3% of the maternal deviance in *rpoS* expression and 67.1% for the constitutive reporter.

In contrast, daughter cells exhibited a homogeneous distribution of intracellular fluorescence (Fig. 4A), with slightly lower fluorescence levels around the old pole area of raw transects (fig. S6 and table S2). Our generalized additive models indicated a significant difference between new and old cell areas ($P < 0.001$), with mean fluorescence varying across cell length ($P < 0.001$) and over time ($P < 0.001$). This means that even the youngest of old poles are slightly darker than new poles, suggesting that intracellular asymmetry might appear quickly as the old pole matures. However, these factors explained a lower fraction of gene expression deviance in daughter cells (*rpoS*: 11.7% and constitutive: 33.3%).

This intracellular asymmetry persisted throughout each cell cycle (Fig. 4, C and D), with the fission plane becoming visible halfway through the generation. The intracellular asymmetry that an individual exhibited before division was correlated with the asymmetry among its offspring (fig. S7), indicating that this pattern propagates across generations. This suggests that the asymmetry in product inheritance, shown in Fig. 2, derives from the intracellular asymmetry that progressively develops within mother cells across generations, with aging affecting the contribution of old poles to total gene expression.

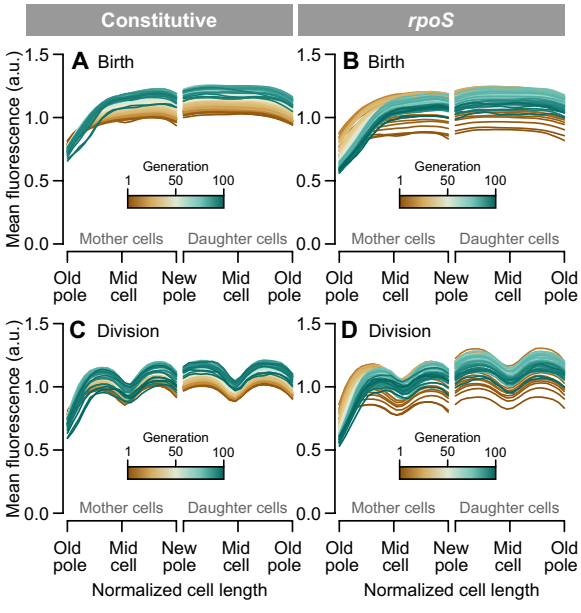

Fig. 4. Gene expression asymmetry across the cell length. Each line represents a series of fluorescence measurements from pole to pole, averaged for all cells of a given generation. For both promoters, mother cells had darker areas around the old poles from birth (**A** and **B**) to division (**C** and **D**), indicating a gradient in gene expression along the cell length. Daughter cells, on the other hand, showed higher intracellular homogeneity in gene expression. The fission site was visible in the transects measured before division. Control analyses and transformations to avoid positioning artifacts are detailed in Supplementary Text and fig. S5. These results suggest that the asymmetry between mother and daughter after division (Fig. 2B) derives from the intracellular gradient built within the mother cell over time (see also fig. S6).

Pole age determines intracellular gene expression asymmetry

Since mother cells exhibit an intracellular gradient (Fig. 4) and product inheritance asymmetry increases over time (fig. S3), we hypothesize that maternal intracellular heterogeneity is age dependent. In rod-shaped bacteria, age is a function of how many times a cell pole was consecutively inherited. While maternal old poles exist for up to 100 generations in our experiments ($0 < age \leq 100$), their new poles are always synthesized at the last fission event ($age = 0$). The new pole of the daughter cell, consequently, also has $age = 0$, while its old pole has $age = 1$. Hence, we expect old poles of mother cells to be physiologically older, while new poles of mothers and daughters should be equivalent. If fluorescence gradients develop as a progressive effect of aging, then intracellular asymmetry should be a function of the age difference between new and old cell poles at a given generation.

This is demonstrated through fluorescence measurements in Fig. 5. For both reporters, maternal old poles exhibited lower GFP accumulation than old poles of daughter cells (Fig. 5A). Fluorescence levels in new poles, on the other hand, showed a small albeit significant difference between mothers and daughters (Fig. 5B). The greater homogeneity of daughter cells can also be visualized through the ratios between new and old poles, which provides a measurement of intracellular asymmetry (Fig. 5C). Daughter intracellular ratios approached 1, showing little change over time (constitutive: $slope = 0.02$ and *rpoS*: $slope = 0.09$), since the age of both poles remains constant for daughter cells. Mother cells, in contrast, exhibited increasing intracellular asymmetry with each division (constitutive: $slope = -0.26$ and *rpoS*: $slope = -0.57$), which coincides with the increasing age difference between maternal old and new poles.

The mother machine design allows us to extend this analysis to the subsequent pair of cells, represented in fig. S8. When a daughter cell divides, its old and new poles age by one generation as they are inherited by the offspring. Daughter 2 inherits the new pole, now *age* = 1, while daughter 3 receives the old pole (*age* = 2). It is important to look at these cells to determine how quickly intracellular asymmetry is built across generations, i.e., whether the lapse of a single generation can produce physiological asymmetry between cell poles. Our results confirmed that daughter 3 displays lower fluorescence levels in its old pole (new versus old pole paired *t* test: $t = 132.5$ and $P < 0.001$), thus exhibiting intracellular asymmetry (fig. S8). Furthermore, since daughter 3 is positioned closer to the opening of the growth well and surrounded by neighboring cells, its asymmetry supports the idea that this phenomenon has a physiological origin rather than being an imaging artifact.

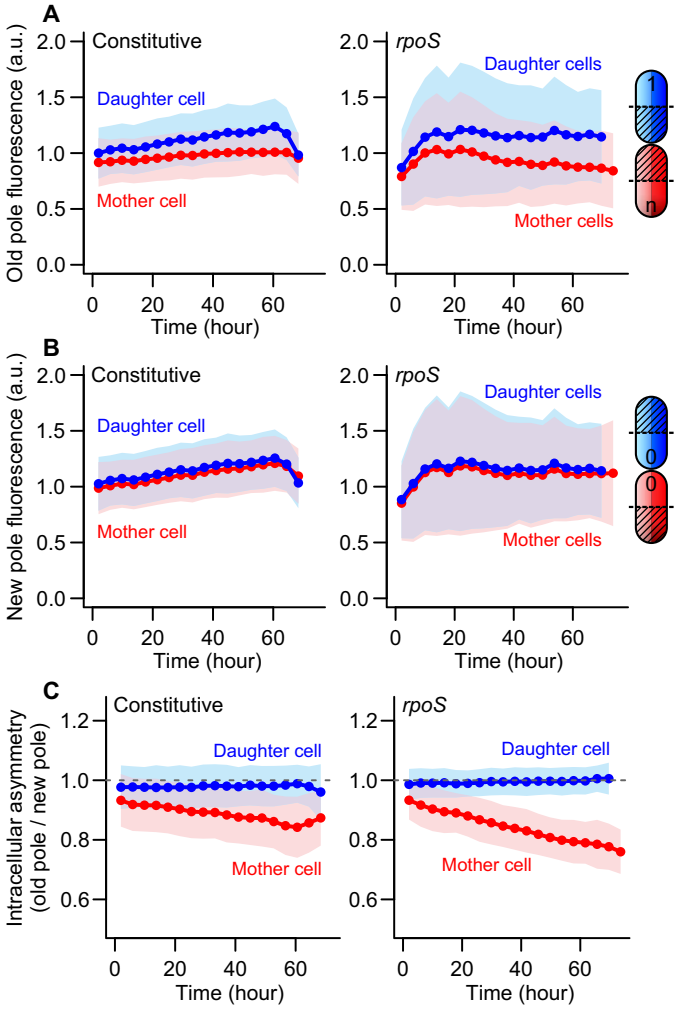

Fig. 5. Intracellular asymmetry depends on the age of cell poles. For lineages in a mother machine device, maternal old poles become older with each generation ($1 < age \leq 100$), while old poles of daughter cells always have age = 1. This difference in pole ages predicts that most of the difference between mother and daughter cells should come from their old poles. (**A**) Fulfilling this prediction, we verified that old poles of daughter cells exhibited higher fluorescence expression than maternal old poles for both constitutive (paired *t* test: $t = 77.50$, $n = 31,257$, and $P < 0.001$) and *rpoS* ($t = 50.79$, $n = 18,444$, and $P < 0.001$) reporters. (**B**) In contrast, new poles of mother and daughter cells showed little difference in gene expression (paired *t* test; constitutive: $t = 22.57$, $n = 31,257$, and $P < 0.001$; and *rpoS*: $t = 10.60$, $n = 18,444$, and $P < 0.001$), since both new poles are generated at the fission site. (**C**) The age difference between new and old poles increases over time for mother cells, leading to an increase in intracellular asymmetry as the mother ages. Daughter cells remain nearly symmetric over time, coinciding with a constant age difference between poles. [(A) to (C)] Bins = mean ± SD.

Together, these results suggest that gene expression gradients across each cell depend on the difference in age between its new and old cell poles. We verified that intracellular asymmetry develops independently of extrinsic stress, such as photooxidation produced by imaging (fig. S9), thus representing an intrinsic aspect of bacterial physiology. Therefore, these findings indicate that old poles have a progressive decline in product concentrations, which could be due to age-specific changes in diffusion operating differently in new and old poles (*28*). Intracellular gradients can be found in any cell inheriting an old pole, and become more pronounced as the cell ages. The progressive development of these gradients could be due to the gradual accumulation of other components in old cell poles, such as protein aggregates (*32*) or efflux pumps (*54*), both of which have also been associated with slower maternal growth. As this process determines mother-daughter asymmetry upon division, this pattern then propagates across generations.

Morphological asymmetry emerges with maternal aging

To assess whether the decline in old pole activity impacts cell growth, we evaluated the extent of the maternal cell influenced by this decline. We estimated the length of maternal old poles based on *rpoS* expression gradients (Fig. 4, A and B). For each cell, we performed a segmented regression analysis to identify the transition point between the polar gradient and the fluorescence plateau. The distance from the cell pole to this breakpoint represents the cell length that is affected by aging, which can be considered as the "old pole length" (Fig. 6A).

We found that the old pole length increased over time ($slope = 0.14$ and $P < 0.001$), which would be expected from our previous observations. Not only do fluorescence levels at this end of the cell decrease, but a longer area of the mother cell is subjected to this decline as it ages. This was accompanied by an overall increase in cell length over time ($slope = 0.18$ and $P < 0.001$), although at a distinct rate from the old pole length (ANCOVA interaction: $F = 87.08$ and $P < 0.001$). Combining these measurements, we observed an increase in the fraction of the mother cell represented by the old pole, going from 25.3 to 36.2% after ~100 generations (Fig. 6B). Because the increasing maternal length is not reflected in the daughter, a morphological asymmetry between mothers and daughters developed over time (Fig. 6C). When we recalculated *rpoS* activity estimates while excluding the maternal old pole area (Fig. 6, D and E), we observed that both mean fluorescence (paired *t* test: $t = 28.31$, $n = 18,979$, and $P < 0.001$) and promoter activity ($t = 164.58$, $n = 18,979$, and $P < 0.001$) increased, approaching daughter cell levels. This suggests that aging effects are mostly bound to the old pole area, reinforcing the observations that physiological asymmetry is determined by the inheritance of old poles. The fact that promoter activity remained asymmetric despite the removal of old poles indicates that other factors, such as metabolic rates, might remain an essential component of bacterial asymmetry.

Our results demonstrate that the gradual increase in maternal intracellular asymmetry is accompanied by a progressive increase in cell length. This gradual elongation derives from off-center divisions leading

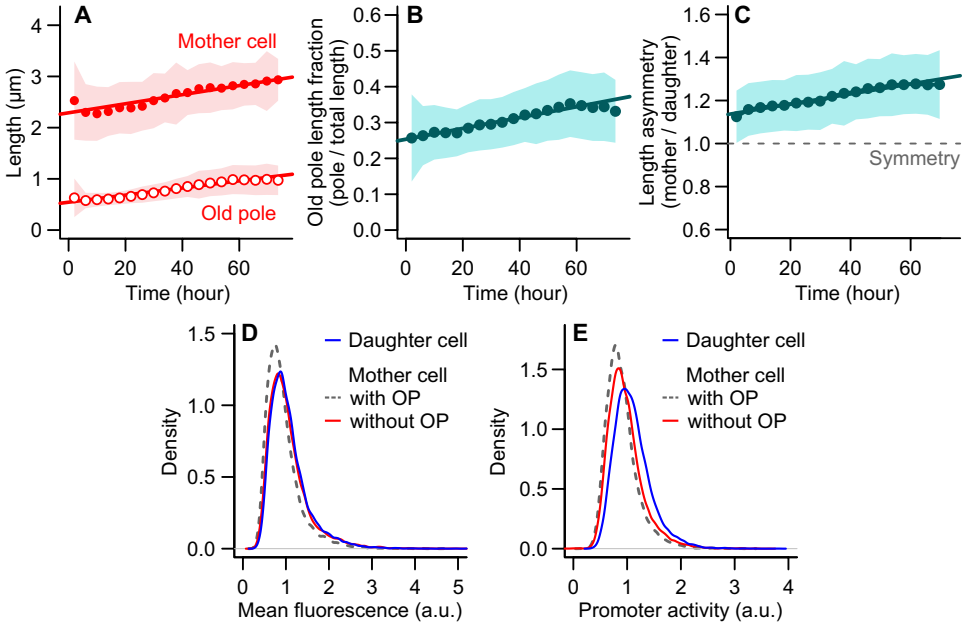

Fig. 6. Lengthening of the old pole contributes to decline in gene expression. (**A**) Mother cells increase in birth length over time, which is accompanied by an elongation of the old pole area of the cell. (**B**) With age, old poles represent an increasingly larger proportion of the mother cell (*slope* = 0.0015, $t = 50.82$, and $P < 0.001$). (**C**) Since daughter cells carry old poles of a constant age, the morphological asymmetry between mothers and daughters increases over time (*slope* = 0.0023, $t = 51.95$, and $P < 0.001$). This suggests that aging in *E. coli* is not just a matter of physiological asymmetry but also comprises a morphological asymmetry that develops as the mother ages. [(A) to (C)] Bins = mean ± SD. (**D** and **E**) If we remove the old pole area of the mother cells and re-estimate mean fluorescence and *rpoS* promoter activity, these measurements approach the levels of daughter cells. This suggests that bearing old poles contributes to the lower gene expression observed in mother cells.

to the emergence of morphological asymmetry, which could be similar to the FtsZ ring displacement previously observed in cells containing protein aggregates (*55*). Together, these results indicate that increasingly aged old poles promote a gradual decline in maternal gene expression, producing intracellular asymmetry gradients that are propagated across generations. Through divisional asymmetry, bacterial aging contributes to enhance not only the heterogeneity in *E. coli* growth rates but also in gene product inheritance, gene expression, and cell length.

DISCUSSION

Although bacterial growth and gene expression are highly stochastic, part of this variability can be explained by aging processes. We showed that mother cells have lower gene expression rates than their daughters (Figs. 2 and 3), independently of whether the activity of a given promoter was positively or negatively correlated with growth. Asymmetry was present even when mothers and daughters elongated at similar rates (Fig. 3B), indicating that this phenomenon cannot be explained by the higher metabolic rates of daughter cells but rather by cellular aging. As the mother ages, it develops an intracellular asymmetry gradient due to the increasing age difference between its old and new poles (Figs. 4 and 5), which manifests in the next generation as the asymmetry between mother and daughter. The daughter cell, which has poles of similar age, exhibits homogeneous gene expression. Last, we showed that maternal aging also leads to morphologically asymmetric divisions (Fig. 6). These results indicate that aging processes contribute to increase phenotypic heterogeneity within bacterial populations, encompassing both physiological aspects, such as growth, product partitioning, and gene expression, as well as morphological aspects.

A comparable paradigm shift occurred when previous studies demonstrated the influence of aging over the distribution of bacterial growth states. Although bacteria grow at a constant rate when maintained in stable environmental conditions (*45*, *56*), mother and daughter cells reach distinct states of growth stability (*10*), building on the notion that the inheritance of old cell poles leads to lower fitness (*20*, *21*, *32*). This deterministic asymmetry can be advantageous over the purely stochastic partitioning of damaged components (*9*, *27*). Nonetheless, stochastic components have a core relevance for bacterial physiology, dictating mortality patterns of mother and daughter cells (*11*), and propagating through genetic regulatory networks (*1*, *2*). One example of a highly stochastic component is the sigma factor RpoS, whose pulsating dynamics of growth inhibition can lead to higher stress survival (*4*, *8*, *57*). By showing that mother and daughter cells have asymmetric *rpoS* expression, our results suggest yet another layer to the phenotypic heterogeneity modulated by aging. It remains an open question whether the higher levels of RpoS observed in daughter cells could also be involved in their higher probability of survival to oxidative stresses (*25*).

The evidence that asymmetry is also present at the gene expression level also invites a new mechanistic perspective on bacterial aging that links molecular to organismal processes. For instance, Shi *et al.* (*43*) demonstrated that daughter cells receive more newly synthesized proteins upon division, although this study could not determine long-term aging dynamics. Our results suggest that asymmetry is built into the mother cell over time, through an age-associated decline in old pole physiology. At the molecular level, it is possible that efflux pumps, segregated asymmetrically toward old poles (*54*), might contribute to creating an intracellular protein gradient. Moreover, we show that bacterial asymmetry extends beyond the simple inheritance of genetic

products, with daughter cells exhibiting higher rates of gene expression. Although this might be partly explained by the fact that ribosomes are also partitioned asymmetrically (*51*), gene expression asymmetry is present even after correcting for differences in growth rates, which are highly correlated with ribosomal content (*50*, *58*). Similarly, the subcellular localization of ribosomes is driven by nucleoid occlusion (*35*, *59*), this phenomenon does not determine the asymmetric distribution of proteins (*28*). It is likely that a combination of factors, from the inheritance of newly synthesized components to the accumulation of damaged proteins, interacts to produce the progressive decline we report.

The maternal aging phenotype has been traditionally attributed to the accumulation of misfolded proteins (*32*, *36*), which is determined by the nucleoid mesh size (*34*, *35*). However, recent studies have suggested that the inheritance of protein aggregates does not correlate with slower elongation rates (*40*, *41*). It is important noting, nonetheless, that whether or not the accumulation of protein aggregates in the old poles is correlated with a decline in growth, it could affect other physiological processes. Aggregates have the potential for decreasing protein diffusion rates (*28*), producing differential rates in new and old cell poles. We do not discard the possibility that such aggregates might promote the formation of intracellular gradients in mother cells. Furthermore, the pole-associated aggregates can displace the FtsZ ring and generate morphological asymmetry upon division (*55*), which would explain the increase in maternal length with age (Fig. 6). It is therefore possible that mother cells accumulate misfolded proteins as they age, which would lead to a progressive displacement of ribosomes and gene products away from old poles. At the same time, the displacement of the FtsZ ring and consequent increase in maternal length might compensate for any negative effects of damage accumulation, thus allowing for elongation rates to remain stable. Nonetheless, since the accumulation of large aggregates is a rare occurrence among unstressed cells (*40*), further studies are necessary to investigate the correlation between protein aggregation, growth, and gene expression across generations.

We have shown that cellular aging contributes to the phenotypic heterogeneity found within bacterial populations, influencing growth and gene expression. More than producing a fixed asymmetry between mothers and daughters, the progressive aging of old poles widens the physiological heterogeneity with each division. By linking gene expression and aging dynamics, our findings provide a framework for future studies on the causal understanding of bacterial aging. Moreover, our results invite the question of which other mechanisms of metabolic regulation might be involved in the aging process. It is possible that the maturation and physiological decline of the old poles have direct consequences for bacterial growth, e.g., the old area, representing a considerable fraction of the mother cell, might have a lower contribution to cell wall elongation, producing differences in elongation rates among mother and daughter cells. Together, our findings demonstrate that cellular aging is an essential part of nongenetic variance in bacterial populations, and future studies might elucidate its role as a driver of phenotypic heterogeneity involved with survival to oxidative stress and antibiotic treatments.

MATERIALS AND METHODS

Strains and growth conditions

E. coli K-12 strain MG1655 containing a plasmid-based GFP reporter of RpoS expression was obtained from the U. Alon library (*46*). Extensive characterizations of reporters in this library, including of RpoS and downstream promoters, demonstrated that activity patterns observed on a plasmidial reporter do not differ from a chromosomally integrated one, except for a lower fluorescence intensity of the latter (*4*, *8*, *44*). We have corroborated this observation for our analyses on intracellular asymmetry (fig. S10). Reporters from this library have also been shown to match biological expression levels (*60*). Since imaging strains with a chromosomal integration would require higher exposure to phototoxic stress, we used the original strain to minimize damage exposure. *RpoS* expression patterns were compared with constitutive GFP expressed under the PA1 promoter (*47*). Liquid cultures were performed on M9 minimal media (1xM9 salts, 2 mM $MgSO_4$, and 0.1 mM $CaCl_2$) supplemented with 0.2% casamino acids and 0.4% glucose. For microfluidic experiments, 0.075% Tween 20 (Sigma-Aldrich) and propidium iodide (PI; 1 μg/ml) were added to the media. Tween 20 prevents cell adhesion to the walls of a microfluidic device, and PI is a marker of cell lysis. All experiments were conducted at 37°C.

Microfluidic design and fabrication

The mother machine microfluidic design was used for cell capture and single-cell imaging (*45*). The design consisted of four parallel flow channels (1 cm × 80 μm × 10 μm), each containing 1000 growth wells (25 × 0.8 × 1.2 μm). Each growth well contains a mother cell lineage, which receives fresh culture medium diffused from the flow channels throughout the experiment. The original mold was fabricated through laser etching, and epoxy copies were produced for constant handling. Individual devices were fabricated with Sylgard 184 polydimethylsiloxane (PDMS) (Dow Corning, USA) using epoxy copies as negative molds for PDMS casting. The cast was degassed in a vacuum chamber and hardened at 80°C for 1 hour, then removed from the mold and punctured with a 0.5-mm biopsy punch to create inlet and outlet ports. Each device was thoroughly washed with ethanol and water, dried, and attached to 24 × 40 mm coverslips through plasma bonding. A final curing step was performed by incubating bonded devices at 60°C overnight. Before use, devices were plasma activated and treated with 20% polyethylene glycol for 1 hour.

Cell loading and device setup

Overnight bacterial cultures were diluted 1:100 into 15 ml of M9 media and grown to exponential phase for 2 hours before loading (until optical density at 600 nm = 0.4 to 0.6 was reached). Cultures were centrifuged at 4000 rpm for 10 min, then resuspended into 200 μl of M9 + Tween 20 + PI. These concentrated cultures were injected into the devices through the outlet ports, and devices were centrifuged at 1500 rpm for 8 min to push bacteria into the growth wells. Once the proper loading was verified, the flow media input was connected to each device through Tygon tubing (ND 100-80, Saint-Gobain, Darwin Microfluidics). A constant flow of 200 μl/hour was ensured by a peristaltic pump (Ole Dich, Denmark). In the segment of the inlet tubing that ran through the pump, Tygon tubing was replaced by flexible pumping tubing (Masterflex Tygon E-3603, VWR). Outflow tubing were connected to outlet ports, running to a waste container. Loaded devices were placed in the microscopy incubation chamber at 37°C (PeCon TempController 2000-1). Each microfluidics experiment was performed in duplicates.

For stationary phase experiments (fig. S2), this setup was combined with an inlet of spent M9 medium. An overnight culture was grown in M9, which was then centrifuged and filter sterilized. This spent medium was supplemented with 0.075% Tween 20 and PI (1 μg/ml)

and connected to the regular media inlet with a replacement rate of 600 µl/hour.

Microscopy and image acquisition

Time-lapse imaging was performed on a Nikon Eclipse Ti2 inverted microscope equipped with a motorized stage and perfect focus system, using a 100× oil objective and DS-Qi2 camera. Automated image acquisition was controlled through the NIS Elements software, configured for phase contrast acquisition in 2-min intervals for 72 hours. To decrease photooxidation effects (*25*), images for green (460 nm) and red (550 nm) fluorescence quantification were obtained in 10-min intervals. The exposure and intensity of fluorescence imaging were adapted for each promoter to induce minimal stress while ensuring signal detection (*rpoS*: green = 200 ms, 1%; and red = 300 ms, 2%; and constitutive: green = 150 ms, 4%; and red = 150 ms, 8%).

Image processing

Images were pre-processed on ImageJ for chromatic shift correction and background subtraction (rolling ball radius = 20 px, sliding paraboloid). Through the ZEDAT High-Performance Computer resources at FU Berlin (*61*), automated image processing for cell segmentation and tracking was performed using the DeLTA deep learning–based software (*62*), for which the deep learning algorithm was further trained on diverse single-cell data from our experimental system. Segmentation was performed on phase contrast images, and measurements were obtained for cell length, area, division intervals, and mean fluorescence intensity. Fluorescence transects were obtained by extracting the mean fluorescence intensity of each pixel along the mid-cell line. Segmentation and tracking errors, although rare, were corrected with a custom program implemented in R version 4.1.2 (*63*). Manual corrections were performed when necessary. Each lineage was followed until the death of the mother cell, determined by the appearance of PI signal in red fluorescence images. Only complete generations were considered for statistical analyses (i.e., daughter cells that left the growth well before a division was observed were excluded from measurements).

Statistical analysis

Statistical analyses on the output growth and fluorescence data were performed in R version 4.1.2, considering mother cells for the entirety of the experiments and the first generation of each daughter cell. For the comparison of individuals at the same stage of the cell cycle, fluorescence measurements were taken from the first frame after division (indicated as "birth" frame on Fig. 4), unless otherwise indicated. Elongation rates were calculated for each cell from an exponential fit to length measurements of each generation. As such, mean fluorescence and elongation rate estimates for mothers and daughters are paired for every division. When parametric tests on fluorescence data were necessary, the data were log-transformed to ensure normal distribution of residuals. Figure 3B plots were made using R packages "ggplot2"and "ggdensity" to outline highest density regions of elongation rates and promoter activity distributions (*64*, *65*). On representations of binned data, bins represent mean ± SD, and bins comprising fewer than 10 measurements were excluded. The only exception is Fig. 2D, whose bins represent mean ± SE as indicated in the figure legend.

Fluorescence transects shown in Fig. 4 were normalized by length for graphical representation and for analysis through generalized additive models, which were performed using R package mgcv version 1.3-38 (*66*). Generalized additive models are well suited for the comparison of complex nonlinear models, as splines are fitted using interpolation of local piecewise polynomials (*66*). While the transects in the main figure were averaged for each generation, individual measurements were used in the analysis. We focused on the differences between new and old cell areas for the construction of the models, as shown in table S2 (see also fig. S6, A and B). Each fluorescence transect was cut in half, thus splitting the new and old areas of each cell, and the distance from the pole toward the center was used as a smoothing term in the model. The model structure that provided the lowest Akaike information criterion (AIC) was considered as the preferred model (table S2) (*67*). We chose AIC over other information theoretic approaches (e.g., Bayesian information criterion) as AIC is less influenced by sample size. Transects shown in Fig. 4 were cropped on both ends before length normalization, to avoid positioning artifacts described in Supplementary Text and fig. S5. Cropped transects were used in analyses shown in Fig. 5 and fig. S6 (C and D). On analyses quantifying pairwise differences in intracellular asymmetry, such as in Fig. 5, fluorescence transects were used without the need for length normalization.

Nonnormalized transects were also used to obtain the proportion of the mother cell represented by the old area, shown in Fig. 6. In this case, each log-transformed transect was fitted with a segmented regression using R package "segmented" version 1.4-0 (*68*). The segmented regression analysis identifies the breakpoint along the cell length where a linear fit to the gradient transitions into a fluorescence plateau. This breakpoint was used as the old pole length (end of gradient) in further analyses.

Promoter activity quantification

The estimate of *rpoS* promoter activity was performed as previously described (*4*, *8*). Given the mean fluorescence of a cell (M), its length (L) and a constant ($P = 0.02$), promoter activity (A) is defined as

$$A = M\left(\frac{1}{L}\frac{dL}{dt} + p\right) + \frac{dM}{dt}$$

The promoter activity of mother cells over time (fig. S1) was calculated for all fluorescence measurements throughout the individual's lifespan. In this case, M was smoothed with a moving window of five fluorescence frames, and the resulting A was again averaged over a similar moving window for graphical representation. dL/dt and dM/dt were estimated as the difference between consecutive frames containing fluorescence images (every 10 min). For the comparison of mother and daughter cells (Fig. 3), since the latter was only followed for a generation, measurements (M and L) at the beginning and end of each generation were used to obtain A. The time interval, in this case, corresponded to the division interval. No data smoothing was used in this comparison.

Supplementary Materials

The PDF file includes:

Supplementary Text
Figs. S1 to S10
Tables S1 to S3
Legend for movie S1

Other Supplementary Material for this manuscript includes the following:

Movie S1

REFERENCES AND NOTES

1. A. Urchueguía, L. Galbusera, D. Chauvin, G. Bellement, T. Julou, E. van Nimwegen, Genome-wide gene expression noise in *Escherichia coli* is condition-dependent and

determined by propagation of noise through the regulatory network. *PLOS Biol.* **19**, e3001491 (2021).
2. N. Rosenfeld, J. W. Young, U. Alon, P. S. Swain, M. B. Elowitz, Gene regulation at the single-cell level. *Science* **307**, 1962–1965 (2005).
3. C. Wu, R. Balakrishnan, N. Braniff, M. Mori, G. Manzanarez, Z. Zhang, T. Hwa, Cellular perception of growth rate and the mechanistic origin of bacterial growth law. *Proc. Natl. Acad. Sci. U.S.A.* **119**, e2201585119 (2022).
4. O. Patange, C. Schwall, M. Jones, C. Villava, D. A. Griffith, A. Phillips, J. C. W. Locke, *Escherichia coli* can survive stress by noisy growth modulation. *Nat. Commun.* **9**, 5333 (2018).
5. N. Q. Balaban, J. Merrin, R. Chait, L. Kowalik, S. Leibler, Bacterial persistence as a phenotypic switch. *Science* **305**, 1622–1625 (2004).
6. O. Gefen, N. Q. Balaban, The importance of being persistent: Heterogeneity of bacterial populations under antibiotic stress. *FEMS Microbiol. Rev.* **33**, 704–717 (2009).
7. P. B. Rainey, H. J. Beaumont, G. C. Ferguson, J. Gallie, C. Kost, E. Libby, X.-X. Zhang, The evolutionary emergence of stochastic phenotype switching in bacteria. *Microb. Cell Fact.* **10**, S14 (2011).
8. N. M. V. Sampaio, C. M. Blassick, V. Andreani, J.-B. Lugagne, M. J. Dunlop, Dynamic gene expression and growth underlie cell-to-cell heterogeneity in *Escherichia coli* stress response. *Proc. Natl. Acad. Sci. U.S.A.* **119**, e2115032119 (2022).
9. L. Chao, C. U. Rang, A. M. Proenca, J. U. Chao, Asymmetrical damage partitioning in bacteria: A model for the evolution of stochasticity, determinism, and genetic assimilation. *PLOS Comput. Biol.* **12**, e1004700 (2016).
10. A. M. Proenca, C. U. Rang, C. Buetz, C. Shi, L. Chao, Age structure landscapes emerge from the equilibrium between aging and rejuvenation in bacterial populations. *Nat. Commun.* **9**, 3722 (2018).
11. U. K. Steiner, A. Lenart, M. Ni, P. Chen, X. Song, F. Taddei, J. W. Vaupel, A. B. Lindner, Two stochastic processes shape diverse senescence patterns in a single-cell organism. *Evolution* **73**, 847–857 (2019).
12. D. Choudhary, V. Lagage, K. R. Foster, S. Uphoff, Phenotypic heterogeneity in the bacterial oxidative stress response is driven by cell-cell interactions. *Cell Rep.* **42**, 112168 (2023).
13. S. C. Stearns, The evolution of life history traits: A critique of the theory and a review of the data. *Annu. Rev. Ecol. Syst.* **8**, 145–171 (1977).
14. M. R. Rose, *Evolutionary Biology of Aging* (Oxford Univ. Press, New York, 1991).
15. T. B. L. Kirkwood, Evolution of ageing. *Nature* **270**, 301–304 (1977).
16. G. C. Williams, Pleiotropy natural selection and the evolution of senescence. *Evolution* **11**, 398–411 (1957).
17. W. D. Hamilton, The moulding of senescence by natural selection. *J. Theor. Biol.* **12**, 12–45 (1966).
18. N. Erjavec, M. Cvijovic, E. Klipp, T. Nyström, Selective benefits of damage partitioning in unicellular systems and its effects on aging. *Proc. Natl. Acad. Sci. U.S.A.* **105**, 18764–18769 (2008).
19. S. R. Laney, R. J. Olson, H. M. Sosik, Diatoms favor their younger daughters. *Limnol. Oceanogr.* **57**, 1572–1578 (2012).
20. M. Ackermann, S. C. Stearns, U. Jenal, Senescence in a bacterium with asymmetric division. *Science* **300**, 1920 (2003).
21. E. J. Stewart, R. Madden, G. Paul, F. Taddei, Aging and death in an organism that reproduces by morphologically symmetric division. *PLOS Biol.* **3**, e45 (2005).
22. L. Partridge, N. H. Barton, Optimally, mutation and the evolution of ageing. *Nature* **362**, 305–311 (1993).
23. C. U. Rang, A. Y. Peng, L. Chao, Temporal dynamics of bacterial aging and rejuvenation. *Curr. Biol.* **21**, 1813–1816 (2011).
24. L. Jouvet, A. Rodríguez-Rojas, U. K. Steiner, Demographic variability and heterogeneity among individuals within and among clonal bacteria strains. *Oikos* **127**, 728–737 (2018).
25. A. M. Proenca, C. U. Rang, A. Qiu, C. Shi, L. Chao, Cell aging preserves cellular immortality in the presence of lethal levels of damage. *PLOS Biol.* **17**, e3000266 (2019).
26. M. Tuğrul, U. K. Steiner, Demographic consequences of damage dynamics in single-cell ageing. bioRxiv 538602 (2023). https://doi.org/10.1101/2023.05.23.538602.
27. S. N. Evans, D. Steinsaltz, Damage segregation at fissioning may increase growth rates: A superprocess model. *Theor. Popul. Biol.* **71**, 473–490 (2007).
28. D. Linnik, I. Maslov, C. M. Punter, B. Poolman, Dynamic structure of *E. coli* cytoplasm: Supramolecular complexes and cell aging impact spatial distribution and mobility of proteins. *Commun. Biol.* **7**, 508 (2024).
29. T. B. L. Kirkwood, Understanding ageing from an evolutionary perspective. *J. Intern. Med.* **263**, 117–127 (2008).
30. L. Chao, A model for damage load and its implications for the evolution of bacterial aging. *PLOS Genet.* **6**, e1001076 (2010).
31. M. Ackermann, L. Chao, C. T. Bergstrom, M. Doebeli, On the evolutionary origin of aging. *Aging Cell* **6**, 235–244 (2007).
32. A. B. Lindner, R. Madden, A. Demarez, E. J. Stewart, F. Taddei, Asymmetric segregation of protein aggregates is associated with cellular aging and rejuvenation. *Proc. Natl. Acad. Sci. U.S.A.* **105**, 3076–3081 (2008).
33. A. B. Lindner, A. Demarez, Protein aggregation as a paradigm of aging. *Biochim. Biophys. Acta Gen. Subj.* **1790**, 980–996 (2009).
34. A. S. Coquel, J. P. Jacob, M. Primet, A. Demarez, M. Dimiccoli, T. Julou, L. Moisan, A. B. Lindner, H. Berry, Localization of protein aggregation in *Escherichia coli* is governed by diffusion and nucleoid macromolecular crowding effect. *PLOS Comput. Biol.* **9**, e1003038 (2013).
35. Y. Xiang, I. V. Surovtsev, Y. Chang, S. K. Govers, B. R. Parry, J. Liu, C. Jacobs-Wagner, Interconnecting solvent quality, transcription, and chromosome folding in *Escherichia coli*. *Cell* **184**, 3626–3642.e14 (2021).
36. J. Winkler, A. Seybert, L. König, S. Pruggnaller, U. Haselmann, V. Sourjik, M. Weiss, A. S. Frangakis, A. Mogk, B. Bukau, Quantitative and spatio-temporal features of protein aggregation in *Escherichia coli* and consequences on protein quality control and cellular ageing. *EMBO J.* **29**, 910–923 (2010).
37. C. López-Otín, M. A. Blasco, L. Partridge, M. Serrano, G. Kroemer, The hallmarks of aging. *Cell* **153**, 1194–1217 (2013).
38. N. Gregersen, P. Bross, S. Vang, J. H. Christensen, Protein misfolding and human disease. *Annu. Rev. Genomics Hum. Genet.* **7**, 103–124 (2006).
39. D. L. Moore, G. A. Pilz, M. J. Arauzo-Bravo, Y. Barral, S. Jessberger, A mechanism for the segregation of age in mammalian neural stem cells. *Science* **349**, 1334–1338 (2015).
40. S. K. Govers, J. Mortier, A. Adam, A. Aertsen, Protein aggregates encode epigenetic memory of stressful encounters in individual *Escherichia coli* cells. *PLOS Biol.* **16**, e2003853 (2018).
41. U. Łapińska, G. Glover, P. Capilla-Lasheras, A. J. Young, S. Pagliara, Bacterial ageing in the absence of external stressors. *Philos. Trans. R. Soc. Lond. B Biol. Sci.* **374**, 20180442 (2019).
42. D. Steinsaltz, M. D. Christodoulou, A. A. Cohen, U. K. Steiner, *Chance events in aging* (Elsevier Inc., 2019.
43. C. Shi, L. Chao, A. M. Proenca, A. Qiu, J. Chao, C. U. Rang, Allocation of gene products to daughter cells is determined by the age of the mother in single *Escherichia coli* cells. *Proc. Biol. Sci.* **287**, 20200569 (2020).
44. O. K. Silander, N. Nikolic, A. Zaslaver, A. Bren, I. Kikoin, U. Alon, M. Ackermann, A genome-wide analysis of promoter-mediated phenotypic noise in *Escherichia coli*. *PLOS Genet.* **8**, e1002443 (2012).
45. P. Wang, L. Robert, J. Pelletier, W. L. Dang, F. Taddei, A. Wright, S. Jun, Robust growth of *Escherichia coli*. *Curr. Biol.* **20**, 1099–1103 (2010).
46. A. Zaslaver, A. Bren, M. Ronen, S. Itzkovitz, I. Kikoin, S. Shavit, W. Liebermeister, M. G. Surette, U. Alon, A comprehensive library of fluorescent transcriptional reporters for *Escherichia coli*. *Nat. Methods* **3**, 623–628 (2006).
47. D.-D. Yang, A. Alexander, M. Kinnersley, E. Cook, A. Caudy, A. Rosebrock, F. Rosenzweig, Fitness and productivity increase with Ecotypic diversity among *Escherichia coli* strains that coevolved in a simple constant environment. *Appl. Environ. Microbiol.* **86**, e00051-20 (2020).
48. H. Weber, T. Polen, J. Heuveling, V. F. Wendisch, R. Hengge, Genome-wide analysis of the general stress response network in *Escherichia coli*: σ^S-dependent genes, promoters, and sigma factor selectivity. *J. Bacteriol.* **187**, 1591–1603 (2005).
49. R. Lange, R. Hengge-Aronis, Identification of a central regulator of stationary-phase gene expression in *Escherichia coli*. *Mol. Microbiol.* **5**, 49–59 (1991).
50. S. Klumpp, Z. Zhang, T. Hwa, Growth rate-dependent global effects on gene expression in bacteria. *Cell* **139**, 1366–1375 (2009).
51. L. Chao, C. K. Chen, C. Shi, C. U. Rang, Spatial and temporal distribution of ribosomes in single cells reveals aging differences between old and new daughters of *Escherichia coli*. *eLife* **12**, RP89543 (2023).
52. H. Bremer, P. P. Dennis, "Modulation of chemical composition and other parameters of the cell by growth rate" in *Escherichia coli and Salmonella*, F. C. Neidhardt, Ed. (ASM Press, Washington, D.C., 1996), pp. 1553–1569.
53. M. Schaechter, O. MaalOe, N. O. Kjeldgaard, Dependency on medium and temperature of cell size and chemical composition during balanced growth of *Salmonella typhimurium*. *J. Gen. Microbiol.* **19**, 592–606 (1958).
54. T. Bergmiller, A. M. C. Andersson, K. Tomasek, E. Balleza, D. J. Kiviet, R. Hauschild, G. Tkačik, C. C. Guet, Biased partitioning of the multidrug efflux pump AcrAB-TolC underlies long-lived phenotypic heterogeneity. *Science* **356**, 311–315 (2017).
55. J. Mortier, S. K. Govers, A. Cambré, R. Van Eyken, J. Verheul, T. den Blaauwen, A. Aertsen, Protein aggregates act as a deterministic disruptor during bacterial cell size homeostasis. *Cell. Mol. Life Sci.* **80**, 360 (2023).
56. S. Taheri-Araghi, S. Bradde, J. T. Sauls, N. S. Hill, P. A. Levin, J. Paulsson, M. Vergassola, S. Jun, Cell-size control and homeostasis in bacteria. *Curr. Biol.* **25**, 385–391 (2015).
57. Y. Yang, A. L. Santos, L. Xu, C. Lotton, F. Taddei, B. Lindner, Temporal scaling of ageing as an adaptive strategy of *Escherichia coli*. *Sci. Adv.* **5**, eaaw2069 (2019).
58. L. K. Poulsen, T. R. Licht, C. Rang, K. A. Krogfelt, S. Molin, Physiological state of *Escherichia coli* BJ4 growing in the large intestines of streptomycin-treated mice. *J. Bacteriol.* **177**, 5840–5845 (1995).
59. Q. Chai, B. Singh, K. Peisker, N. Metzendorf, X. Ge, S. Dasgupta, S. Sanyal, Organization of ribosomes and nucleoids in *Escherichia coli* cells during growth and in quiescence. *J. Biol. Chem.* **289**, 11342–11352 (2014).

60. L. Wolf, O. K. Silander, E. van Nimwegen, Expression noise facilitates the evolution of gene regulation. *eLife* **4**, e05856 (2015).
61. L. Bennett, B. Melchers, B. Proppe, "Curta: A general-purpose high-performance computer at ZEDAT, Freie Universität Berlin" (2020); http://dx.doi.org/10.17169/refubium-26754.
62. J. B. Lugagne, H. Lin, M. J. Dunlop, DeLTA: Automated cell segmentation, tracking, and lineage reconstruction using deep learning. *PLOS Comput. Biol.* **16**, e1007673 (2020).
63. R Core Team, R: A language and environment for statistical computing (2017); https://www.r-project.org/.
64. H. Wickham, ggplot2: Elegant Graphics for Data Analysis (Springer-Verlag New York, 2016; https://ggplot2.tidyverse.org).
65. J. Otto, D. Kahle, *ggdensity: Interpretable Bivariate Density Visualization with "ggplot2"* (2023; https://jamesotto852.github.io/ggdensity/).
66. S. N. Wood, Fast stable restricted maximum likelihood and marginal likelihood estimation of semiparametric generalized linear models. *J. R. Stat. Soc. Ser. B Stat. Methodol.* **73**, 3–36 (2011).
67. K. P. Burnham, D. R. Anderson, Multimodel inference: Understanding AIC and BIC in model selection. *Sociol. Methods Res.* **33**, 261–304 (2004).
68. V. M. R. Muggeo, Estimating regression models with unknown break-points. *Stat. Med.* **22**, 3055–3071 (2003).

Acknowledgments: We thank the Evolutionary Demography Group members: L. Stäcker and J. Kuom for experimental support, discussions, and feedback; and M. Lajine, V. Flatt, E. Pekuz, and J. Bellmann for contributing with experimental controls and validation. We thank D. Roizman and M. Herzog for providing the constitutive promoter strain. We thank the HPC Service of FUB-IT, Freie Universität Berlin, for computing time. **Funding:** This work was supported by the Rising Star Postdoctoral Fellowship, Freie Universität Berlin (A.M.P.); Humboldt Research Fellowship, Alexander von Humboldt Foundation (A.M.P.); German Research Foundation grant 430174701 (M.T. and A.N.); Marie Skłodowska-Curie Actions' European Postdoctoral Fellowship grant 101069035 (M.T.); and Heisenberg Programme of the German Research Foundation grant 430170797 (U.K.S.). **Author contributions:** Conceptualization: A.M.P. and U.K.S. Data curation: A.M.P. and M.T. Formal analysis: A.M.P. Funding acquisition: A.M.P. and U.K.S. Methodology: A.M.P. and A.N. Investigation: A.M.P. and A.N. Visualization: A.M.P. Software: M.T. Resources: M.T. and U.K.S. Supervision: U.K.S. Writing–original draft: A.M.P. and U.K.S. Writing–review and editing: A.M.P., M.T., A.N., and U.K.S. **Competing interests:** The authors declare that they have no competing interests. **Data and materials availability:** All data needed to evaluate the conclusions in the paper are present in the paper and/or the Supplementary Materials. Additional data and supporting code are available at the Dryad Digital Repository (DOI: 10.5061/dryad.9s4mw6mqg). Strains can be obtained from the Uri Alon library of *E. coli* fluorescent transcriptional reporters (*46*).

Submitted 22 April 2024
Accepted 7 October 2024
Published 8 November 2024
10.1126/sciadv.adp8784